International Journal of Heat and Technology
Vol. 42, No. 2, April, 2024, pp. 414-426
Journal homepage: http://iieta.org/journals/ijht

Analysis of MHD Casson Nanofluid Flow over a Nonlinearly Stretching Surface with Joule Heating, Radiation and Suction Effects

Shaik Jaffrullah[1*], Wuriti Sridhar[1], Ganugapati Raghavendra Ganesh[2]

[1] Department of Mathematics, College of Engineering, Koneru Lakshmaiah Educational Foundation, Vaddeswaram 522302, India
[2] Department of Mathematics, Dhanekula Institute of Engineering & Technology, Vijayawada 521137, India

Corresponding Author Email: sridharwuriti@gmail.com

https://doi.org/10.18280/ijht.420207

Received: 20 December 2023
Revised: 6 March 2024
Accepted: 15 March 2024
Available online: 30 April 2024

Keywords:
Casson nanofluid, chemical reaction, Joule heating, porous medium, radiation effect, non-linear stretching sheet, magnetohydrodynamics (MHD), suction/injection

ABSTRACT

The present study considers MHD Casson nanofluid flow and explore the intriguing effects of suction and injection over a nonlinearly stretched surface through porous media. The Joule heating effect is considered which is the physical process that transforms electrical energy to thermal energy. Nanofluids with definite thermal radiation features can be useful in medical treatments, and energy storage systems, and also can be used as coatings to provide thermal insulation. Nanofluids with chemical reactions have various applications such as the removal of pollutants from water, biomedical field, and catalysts in industrial processes. The chemical reaction is also taken into consideration in this study. The Keller box method is employed to solve the governing equations. Various parameters effects are analysed using graphical representations of concentration, velocity, and temperature. Observing augmented values of porosity, suction/injection, and stretching parameters reveals a decrease in velocity profiles. On the other hand, progressive observations of porosity, Casson, radiation, and Joule heating parameters result in enhanced temperature profiles. Conversely, a reverse trend is observed in the case of nonlinearity and suction/injection constraints. The concentration profile decreases for enhanced observations of heat source parameters. Nusselt number, skin friction, and Sherwood numbers are also calculated. It is witnessed that the skin friction coefficient rises with a higher estimation of the porosity parameter. Nusselt number increases in case of the chemical reaction and nonlinear stretching parameter. Sherwood number decreases for progressive values of chemical reaction and thermophoresis parameters.

1. INTRODUCTION

Many industries require energy-efficient heat transfer of fluids. The only limitation is that thermal conductivity must be low in developing such fluids. So to meet the requirements of industries, a new type of fluid is generated by suspending manometer-sized particles in base fluid [1-5]. Non-Newtonian boundary-layer flows have been the subject of extensive research for several decades due to their wide range of applications in areas such as radial diffusers, thermal oil recovery, and drag reducing agents. Unlike Newtonian fluids, which can be described by a single equation, non-Newtonian fluids exhibit diverse characteristics that cannot be captured by a single model. As a result, various models have been developed to represent the behavior of these fluids. One such model is the Casson fluid model, which has been found to provide more accurate rheological data for many materials compared to other non-Newtonian fluids. Li and Xuan [6] experimented with and investigated nanoparticles' suspension, strangely escalating base fluid's heat exchange behaviour. The heat transmission attribute of a nanofluid escalates by the nanoparticles. Kang et al. [7] clarified the procedure of enhancing of heat conductivity of fluid by using nanoparticles. Jang and Choi [8] discussed various parameters of nanoparticles like volume fraction, Nano unit dimension, and temperature that will describe the heat conductivity of the fluid. Yu et al. [9] reviewed the literature and explained different nanofluids' heat transfer performance. Later, Anoop et al. [10] investigated particle size in the progression of thermal conductivity. They concluded that the mean heat exchange coefficient estimations were augmented with an escalation in the concentration of particle and stream rate.

Casson fluid shows yield stress, and also Casson-type fluid is a pseudoplastic fluid with an extreme thickness at zero shear rates and an elastic limit with no underneath flow. If a shear load is less than the elastic limit operated on the liquid, it performs as a rigid, but if it is more than the elastic limit operated, it initiates progress. Also, Casson nanofluid is particularly useful in cooling of electronic appliances, efficient heat exchanger, drug delivery systems in medical field, processing of food products. Due to these applications Casson nano fluid flow analysis is considered in this study. Dash et al. [11] analysed Casson-type liquid flowing features inside an absorbent medium and noted that flow radius relies on the elastic limit and permeability of the absorbent medium. Hady et al. [12] considered a nanofluid's heat and flow features over

a nonlinear extending sheet. They observed that on increasing the radiation parameter, the nonlinear sheet's stretching parameter 'n' causes a drop in the temperature of nanofluid but grows the heat exchange rates. Nadeem et al. [13] examine Casson-type fluid flow across a sheet, which exponentially shrinks and shows an increment in momentum boundary layer thickness. Mukhopadhyay et al. [14] examine a time-dependent Casson-type fluid stream upon an elongating surface and conclude that greater Casson parameter observations enhance the temperature distribution. Swati [15] discussed Casson fluid movement on the non-linear stretching sheet. The nonlinear stretching parameter will increase the skin friction coefficient. Shehzad et al. [16] studied a Casson-type fluid stream with suction and chemical reaction and found that intensification in the chemical reaction parameter will drop the concentration of the liquid. Afterwards, Mukhopadhyay et al. [17] pondered the Casson-type liquid flowing upon a symmetric wedge. They noticed that the heat conductivity rises with increasing Casson parameter. Pramanik [18] examines Casson fluid movement via extending surface through a porous medium and radiation and detected that increasing the Casson parameter will enhance thermal boundary layer thickness. Sheikholeslami et al. [19] considered the radiation influence on the nanofluid flow and determined that heat transmission grows with the rise in radiation. Haq et al. [20] assumed the stagnant nanofluid movement upon an extending sheet and noticed that the radiation parameter enhances temperature distribution. Hussain et al. [21] scrutinized the Casson-type nanofluid flow within the boundary layer with viscous scatteredness. They concluded that the temperature is boosted by the progressive values of thermophoresis and Brownian motion parameters. Hayat et al. [22] analysed a Casson fluid stream with nanoparticles and observed adaptable heat conductivity enhances temperature. Ibrahim and Makinde [23] studied Casson-type nanofluid movement upon an extending sheet through convective conditions and observed that the drag coefficient escalates with an upsurge in the Casson parameter. Ullah et al. [24] deliberated Casson nanofluid stream over a nonlinear extending sheet with thermal radiation using the Keller box method and concludes increasing values of nonlinear parameter diminishes the velocity of the fluid. Kataria and Patel [25] examined the Casson-type fluid flow along with chemically reactive species and thermal radiative via an upright plate and observed that temperature decays with the growth in the Prandtl quantity. Qing et al. [26] deliberate Casson-type nanofluid movement upon a stretchable surface with a permeable medium and realized that the rapidity outline diminishes for the magnetic parameter. Zaib et al. [27] scrutinized the Casson-type nanofluid upon a plate dipped in a permeable material with activation energy and chemically reactive flow. They concluded that the thickness of the peripheral concentration layer intensifies because of activation energy. After that Naqvi et al. [28] debated the Casson-type nano liquid flowing upon an absorbent extending cylinder, and improved temperature is observed for growing estimations of magnetic and the Casson parameters.

The term joule heating refers to the increase in temperature of a liquid caused by its resistance to electric current in electro kinetic flow. Electric energy derived from a flow of electric current is converted into heat when the current passes through a solid or liquid with finite conductivity. The degree of heat experienced by the conductor material is evidenced by an increase in its temperature. Following the principle of energy conservation, Joule heating can be considered a transformation between electrical energy and thermal energy. Hossain [29] studied free convection flow and observed that the presence of dissipation reduces skin friction and heat conductivity. Later, Chen [30] measured the Joule heating impression upon the fluid flow across an extending surface and noticed that the Joule heating decreases the skin friction coefficient. Afterwards, Hayat and Qasim [31] measured the effect of joule heating along with radiation upon the Maxwell fluid flow using the HAM method. They concluded that the concentration field decreases by increasing the Schmidt number. Bachok et al. [32] investigated the nanofluid flow within the boundary layer and observed that the heat transmission boosts with low estimations of the Prandtl quantity. Chamkha et al. [33] probed the influence of Joule heating, radiative, and chemically reactive species upon free convective fluid flow. They detected that boosting the suction/injection variable reduces drag force. Hayat et al. [34] researched the influence of Joule heating over a radiative surface. They noticed that the rapidity diminishes and skin friction growth for the magnetic parameter. Kempannagari et al. [35] explored the Joule heating effect on the exponentially stretched curved surface. They conclude progressive observations of Eckert number outcomes in growth in temperature. In the analysis of Wakif et al. [36] with the rising observations of thermophoresis enhances the temperature distribution. Later Wakif et al. [37] reported in their study that the stability of the hybrid nanofuid will be significantly enhanced by decreasing the spherical size of nanoparticles. Ganesh and Sridhar [38] measured the influence of the chemically reactive Casson-type nanofluid stream above a moving plate by adaptable thickness. Then, the velocity outline declines for the magnetic, Casson, and permeability parameters. BalajiPrakash et al. [39] explored radiative and heat source impacts on vertical porous plates. They concluded that temperature decreases with the increments in the heat source and Prandtl number. Ganesh and Sridhar [40] examined Casson nanofluid flow across Darcy Forchhiemer porous medium and concluded for incremental values of Prandtl number, both thermal and concentration sketches display a falling tendency. Abo-Dahab et al. [41] analysed Casson type nanofluid flow upon a sheet that is nonlinearly stretched through a porous media. They realized that the temperature diminishes with escalating suction/injection parameter amounts. It is observed in the report of Rasool and Wakif [42] velocity field and the associated boundary layer show incremental trend for enhanced observations of modified Hartman factor. Wakif et al. [43] determined that the Nusselt number, which is proportional to the heat transfer rate, can be reduced by an increase in the Lorentz force. Wakif et al. [44] analysed the stability of nanofluid using Wakif-Galerkin technique and concluded that onset of convection is delayed due to the presence of nanoparticles in the fluid. Gumber et al. [45] demonstrated the buoyancy-driven in the micropolar hybrid nanofluid flow upon an upright surface, considering the suction/injection, magneto force, and thermal radiative effect. They have shown that the injection effect is recommended for better heat transfer. Using the Keller-Box technique, Ganesh et al. [46] computationally investigated the forced convection heat transfer of a magneto-Casson-type liquid in a nonlinear porous medium. Moreover, the mixed convection of Casson liquid has been thoroughly investigated by Sridhar et al. [47]. For incremental observations of Brownian motion argument an enhancing pattern on the concentration of nanoparticles

nearer to elongating sheet is noted for Wakif et al. [48], Later Wakif et al. [49] remarked that the flow speed of nanofluid reduces expressively with the upsurge in the magnetic constraint and also Substantial improvement in the temperature distribution Wakif and Shahb [50] noted in his study that the surface drag force factor can be reduced by reducing the magnetic constraint.

Ghadikolaei and Gholinia [51] discussed Hydrogen specifications on Cu hybrid nanoparticles and mentioned that the shape nanoparticle has a major effect on the growing Nusselt number. Velocity decreases corresponding to greater observations of the Hartman number mentioned by Gulzar et al. [52]. The remarkable improvement in thermal conductivity resulting from the strong hydrogen bonding of hybrid nanofluids has been extensively discussed by Ghadikolaei and Gholina [53]. In their study, they explore the fascinating effects of hydrogen bonding on thermal conductivity, highlighting the significant advancements that can be achieved in this field. Ghadikolaei [54] further provides a comprehensive review of methods for cooling solar PV cells and emphasizes the efficient utilization of renewable resources to mitigate pollution. The effectiveness of cooling is found to be closely correlated with the volume ratio of nanoparticles, as elucidated by Ghadikolaei [55]. In a study conducted by Akbari et al. [56], the non-Fourier heat conduction over a three-dimensional hollow sphere is analyzed using the Cattaneo-Vernotte model. The researchers shed light on the intricacies of heat conduction in this unique geometry, contributing to our understanding of heat transfer phenomena. Siahchehrehghadikolaei et al. [57] propose a model for efficient CPU cooling and suggest that silver heat sinks outperform copper and nickel heat sinks due to their superior heat conductivity. They highlight the potential of silver heat sinks in improving CPU cooling efficiency. Faghiri et al. [58] investigate blood flow through a circular tube and observe that the Nusselt number for shear-thinning blood flow is significantly higher compared to Newtonian fluid flow. This finding has important implications for understanding blood flow dynamics and its implications on heat transfer processes. Rostami et al. [59] investigated dusty hybrid nanofluid flow utilizing RBF technique and observed that for growing observations of the Eckert number temperature of the nanofluid enhances. Attar et al. [60] investigated a novel model to determine the fractional differential equations. Fallah Najafabadi et al. [61] studied nanofluid flow with the RBF method and concludes increasing the Brownian motion parameter enhances the temperature of the fluid. Zangooee et al. [62] studied hybrid nanofluid flow using 5th order RK method, progressive values of thermal slip, and coefficient of heat transfer reduces, Ghadikolaei et al. [63] proposed a model of CGNP/H2O nanofluid flow model for CPU cooling. Hosseinzadeh et al. [64] investigated non-Newtonian fluid flow over a curved stretching surface and noted that Enhancement in heat transfer rate is observed for greater values of Brownian diffusion and thermophoresis.

When comparing the flow of Newtonian nanofluids to Casson nanofluids, it becomes evident that fluid flow over stretched sheets offers enhanced cooling and reduced friction. This phenomenon finds practical applications in various industries, such as aerodynamic extrusion involves the shaping and forming of polymer sheets using the forces and principles of aerodynamics, hot rolling processes, metallic plates cooling, condensation processes with liquid films, and glass-fiber production. Recognizing the significance of fluid flow over stretching sheets, this study investigates the effects of radiation, Joule heating, chemical reactions, suction/injection, and magnetic fields on Casson-type nanofluid flow over a nonlinearly stretched sheet. By analyzing the influence of these parameters, the study aims to gain insights into the behavior and characteristics of Casson nanofluid flow over a non-linear stretching sheet. The findings are presented through graphs that illustrate the impact of MHD (magnetohydrodynamics), Joule heating, radiation, and chemical reaction on the flow dynamics of Casson nanofluids. This research contributes to our understanding of the complex interplay between various factors in nanofluid flow over stretched sheets and provides valuable insights for practical applications in different industries. The validation of the numerical method is observed by calculating local parameters and comparison with previous literature.

2. PROBLEM FORMULATION

This study focuses on investigating the flow characteristics of a two-dimensional, time-independent nanofluid with Casson-type rheology, which is electrically conducting and chemically reactive. The nanofluid flow occurs over a porous sheet that exhibits nonlinear stretchability. The velocity of the flow on the sheet is represented by the equation $u_w = ax^N$, while the temperature is given by $T_w = T_\infty + Ax^N$. Additionally, we investigate the heat transfer mechanisms, including heat generation (sink), thermal radiation, viscous dissipation, and Joule heating. The parameters T_∞ and C_∞ denote the liquid ambient temperature and concentricity, respectively. By analyzing these factors, we aim to gain insights into the behavior and characteristics of the nanofluid flow and heat transfer processes over the stretchable porous sheet (see Figure 1).

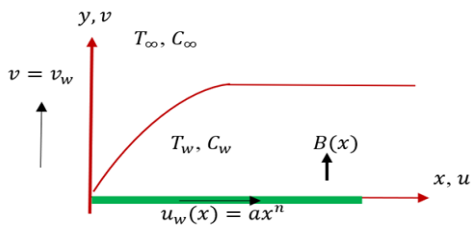

Figure 1. Flow model of the problem

The characteristics of the nanofluid are carefully examined and explained in terms of Brownian diffusion and thermophoretic effects using the Buongiorno model. Like viscous dissipation in viscous fluid flow, joule heating also contributes to heat production. Ejecting heat in various directions to produce materials, manufacture paper, cool electronic chips, and so on. Radiative heat transfer is a critical factor in numerous industries, power generation setups, and high-temperature plasma applications, especially when it comes to managing the heating dynamics of liquid metal fluids and nuclear reactors. With these applications in mind, this paper emphasises on the study of Casson fluid flow upon a nonlinearly heated absorbent media across a stretching surface, considering the involvement of suction/injection, thermal radiation, and Joule heating. The findings of this research have potential applications in fields such as medicine, pharmacology, and chemical industries, among others, where understanding and optimizing heat transfer processes are of

great importance. Based on the hypothesis.

The leading PDEs of the assumed fluid flow given by [32, 41]:

$$v_y + u_x = 0 \tag{1}$$

$$uu_x + vu_y = \upsilon u_{yy} + \left(\frac{\upsilon}{\beta}\right)u_{yy} - \frac{\upsilon}{k_0}u - \frac{\sigma B^2(x)}{\rho_f}u \tag{2}$$

$$\begin{aligned} uT_x + vT_y = {} & \alpha T_{yy} + \frac{Q_0}{\rho c_p}(T - T_\infty) \\ & + \tau\left(\frac{D_T}{T_\infty}\left(\frac{\partial T}{\partial y}\right)^2 + D_B\frac{\partial T}{\partial y}\frac{\partial C}{\partial y}\right) \\ & - \frac{1}{\rho c_p}(q_r)_y + \frac{\sigma B^2(x)}{\rho c_p}u^2 \\ & + \frac{\upsilon}{c_p}\left(1 + \frac{1}{\beta}\right)(u_y)^2 \end{aligned} \tag{3}$$

$$uC_x + vC_y = D_B\frac{\partial^2 C}{\partial y^2} + \frac{D_T}{T_\infty}\frac{\partial^2 T}{\partial y^2} - k_1(C - C_\infty) \tag{4}$$

The proper boundary constraints (BCs) are:

$$\begin{aligned} u = ax^N, v = v_w, D_B\frac{\partial C}{\partial y} + \frac{D_T}{T_\infty}\frac{\partial T}{\partial y} = 0, T = T_w(x) = \\ T_\infty + Ax^N, \text{at } y = 0 \end{aligned} \tag{5}$$

$$u \to 0, T \to T_\infty, C \to C_\infty \text{ as } y \to \infty \tag{6}$$

The similarity conversions [41] are:

$$\left.\begin{aligned} u = ax^N f'(\eta), \\ v = -ax^{\frac{N-1}{2}}\sqrt{\frac{\upsilon}{a}}\frac{N-1}{2}\eta f'(\eta) - ax^{\frac{N-1}{2}}\sqrt{\frac{\upsilon}{a}}\left[\frac{N+1}{2}f(\eta)\right], \\ \eta = \sqrt{\frac{a}{\nu}}x^{\frac{N-1}{2}}y, \\ \theta = \frac{T - T_\infty}{T_w - T_\infty} \\ \phi = \frac{C - C_\infty}{C_w - C_\infty} \end{aligned}\right\} \tag{7}$$

Using transformations mentioned in (7), Eqs. (2)-(4) are transformed to:

$$\left(1 + \tfrac{1}{\beta}\right)f''' + \tfrac{N+1}{2}ff'' - Kf' - Mf' - Nf'^2 = 0 \tag{8}$$

$$\begin{aligned} \left(1 + \frac{4}{3}Rd\right)\theta'' + {} & \frac{N+1}{2}Pr\, f\, \theta' + Pr\, \lambda\, \theta \\ & + Pr\, N\, b\theta'\varphi' + Pr\, N\, t\theta'^2 \\ & + \left(1 + \frac{1}{\beta}\right)Pr\, E\, cf''^2 + Pr\, J\, f'^2 \\ & = 0 \end{aligned} \tag{9}$$

$$\varphi'' + \frac{N+1}{2}Scf\varphi' - Sc\gamma\varphi + \frac{Nt}{Nb}\theta'' = 0 \tag{10}$$

and BCs (5-6) are converted to:

$$\left.\begin{aligned} \text{at } \eta = 0, f = F, f' = 1, \theta = 1, Nb\varphi' + Nt\theta' = 0 \\ as\ \eta \to \infty\ f' \to 0, \theta \to 0, \varphi \to 0 \end{aligned}\right\} \tag{11}$$

where, $M = \frac{\sigma B_0^2}{a\rho_f}$ represents Magnetic parameter, $K = \frac{\upsilon}{ak_0x^{N-1}}$ represents Porous parameter, $Pr = \frac{\upsilon}{\alpha}$ Prandtl number, $Rd = \frac{4\sigma^* T_\infty^3}{kk^*}$ Radiation parameter, $\lambda = \frac{Q_0}{a\rho c_p x^{N-1}}$ represents heat source parameter, $Nb = \frac{\tau D_B(C_w - C_\infty)}{\upsilon}$ represents Brownian motion parameter, $Nt = \frac{\tau D_T(T_w - T_\infty)}{T_\infty \upsilon}$. Thermophoresis parameter, $Ec = \frac{a^2x^{2N}}{C_p(T_w - T_\infty)}$ represents Eckert number, $J = \frac{a\sigma B_0^2 x^{2N}}{\rho c_p(T_w - T_\infty)}$ represents Joule heating parameter, $Sc = \frac{\upsilon}{D_B}$ represents Schmidt number, $\gamma = \frac{k_1}{ax^{n-1}}$ represents chemical reaction parameter.

The local parameters, such as the coefficient of skin friction, Nusselt number, and Sherwood number, are considered as:

$$\begin{aligned} C_{fx} = \frac{\tau_w}{\rho u_w^2}, Nu_x = \frac{xq_w}{\alpha_f(T_w - T_\infty)}, Sh_x \\ = \frac{xq_w}{\alpha_f(T_w - T_\infty)} \end{aligned} \tag{12}$$

where,

$$\begin{aligned} \tau_w = \mu_B\left(1 + \frac{1}{\beta}\right)(u_y)_{y=0}, \quad q_w \\ = -\alpha_f(T_y)_{y=0}, \quad q_m \\ = -D_B(C_y)_{y=0} \end{aligned} \tag{13}$$

Using Eqs. (7) and (12) in (13) we get:

$$\begin{aligned} Re_x^{\frac{1}{2}}C_{fx} = \left(1 + \frac{1}{\beta}\right)f''(0), \\ Re_x^{-\frac{1}{2}}Nu_x = -\left(1 + \frac{4}{3}Rd\right)\theta'(0), \qquad Re_x^{-\frac{1}{2}}Sh_x = -\phi'(0) \end{aligned}$$

3. SOLUTION METHODOLOGY

The non-linear ODE mentioned in Eqs. (8)-(10) was further solved using the Keller box method.

1. First, we convert a set of non-linear ODEs to ODEs of the 1st order.

2. Next, using Newton's scheme, we use finite differences to linearize the system of equations.

3.Furthermore, we obtain a system of linear equations represented in matrix notation.

4. Atlast, the Block tri-diagonal elimination procedure has been applied to Simplify the system. It is solved using MATLAB.

Introducing,

$$f' = p, p' = q, g = \theta, g' = t, s = \phi, s' = n$$

Eqs. (8)-(10) converted to:

$$\left(1 + \frac{1}{\beta}\right)q' + \left(\frac{N+1}{2}\right)fq - Kp - Mp - Np^2 = 0 \tag{14}$$

$$\left(1+\frac{4}{3}Rd\right)t' + \frac{N+1}{2}Pr\,f\,t + Pr\,\lambda\,g + Pr\,N\,btn + Pr\,N\,tt^2 + \left(1+\frac{1}{\beta}\right)Pr\,E\,cq^2 + Pr\,J\,p^2 = 0 \tag{15}$$

$$n' + \frac{N+1}{2}Scfn + \frac{Nt}{Nb}t' - Sc\gamma s = 0 \tag{16}$$

Introducing finite differences,

$$\left.\begin{array}{c}
\frac{1}{h_j}(-f_{j-1}+f_j) = \frac{1}{2}(p_{j-1}+p_j),\\
\frac{1}{h_j}(-p_{j-1}+p_j) = \frac{1}{2}(q_{j-1}+q_j),\\
\frac{1}{h_j}(-g_{j-1}+g_j) = \frac{1}{2}(t_{j-1}+t_j),\\
\frac{1}{h_j}(-s_{j-1}+s_j) = \frac{1}{2}(n_{j-1}+n_j),\\
\left(1+\frac{1}{\beta}\right)\left(\frac{-q_{j-1}+q_j}{h_j}\right)+\left(\frac{N+1}{2}\right)\left(\frac{f_{j-1}+f_j}{2}\right)\left(\frac{q_{j-1}+q_j}{2}\right)-K\left(\frac{p_{j-1}+p_j}{2}\right)\\
-M\left(\frac{p_{j-1}+p_j}{2}\right)-N\left(\frac{p_{j-1}+p_j}{2}\right)^2 = 0,\\
\left(\frac{t_j-t_{j-1}}{h_j}\right)+3\frac{Pr}{3+4Rd}\left(\frac{N+1}{2}\right)\left(\frac{f_j+f_{j-1}}{2}\right)\left(\frac{t_j+t_{j-1}}{2}\right)\\
+\frac{3\lambda Pr}{3+4Rd}\left(\frac{g_j+g_{j-1}}{2}\right)\frac{3\,Pr\,Nb}{3+4Rd}\left(\frac{t_j+t_{j-1}}{2}\right)\left(\frac{n_j+n_{j-1}}{2}\right)\frac{3\,Pr\,N\,t}{3+4Rd}\left(\frac{t_j+t_{j-1}}{2}\right)^2\\
+\frac{3\,Pr\,E\,c}{3+4Rd}\left(\frac{\beta+1}{\beta}\right)\left(\frac{q_j+q_{j-1}}{2}\right)^2+\frac{3\,Pr\,J}{3+4Rd}\left(\frac{p_j+p_{j-1}}{2}\right)^2 = 0,\\
\frac{n_j-n_{j-1}}{h_j}+\left(\frac{N+1}{2}\right)Sc\left(\frac{f_j+f_{j-1}}{2}\right)\left(\frac{n_j+n_{j-1}}{2}\right)+\frac{Nt}{Nb}\left(\frac{t_j-t_{j-1}}{h_j}\right)\\
-Sc\gamma\left(\frac{s_j+s_{j-1}}{2}\right) = 0.
\end{array}\right\} \tag{17}$$

To linearize the equations in (17) using Newton's method, we consider:

$$\left.\begin{array}{l}
f_j^{k+1} = f_j^k + \delta f_j^k,\\
p_j^{k+1} = p_j^k + \delta p_j^k,\\
q_j^{k+1} = q_j^k + \delta q_j^k,\\
g_j^{k+1} = g_j^k + \delta g_j^k,\\
t_j^{k+1} = t_j^k + \delta t_j^k,\\
s_j^{k+1} = s_j^k + \delta s_j^k,\\
n_j^{k+1} = n_j^k + \delta n_j^k.
\end{array}\right\} \tag{18}$$

We make the given below usage of linearly formulas:

$$\left.\begin{array}{c}
\delta f_j - \delta f_{j-1} - \frac{h_j}{2}(\delta p_j) - \frac{h_j}{2}(\delta p_{j-1}) = r_{1,j},\\
\delta p_j - \delta p_{j-1} - \frac{h_j}{2}(\delta q_j) - \frac{h_j}{2}(\delta q_{j-1}) = r_{2,j},\\
\delta g_j - \delta g_{j-1} - \frac{h_j}{2}(\delta t_j) - \frac{h_j}{2}(\delta t_{j-1}) = r_{3,j},\\
\delta s_j - \delta s_{j-1} - \frac{h_j}{2}(\delta n_j) - \frac{h_j}{2}(\delta n_{j-1}) = r_{4,j},\\
a_{1,j}\delta q_j + a_{2,j}\delta q_{j-1} + a_{3,j}\delta f_j + a_{4,j}\delta f_{j-1}\\
+a_{5,j}\delta p_j + a_{6,j}\delta p_{j-1} = r_{5,j},\\
b_{1,j}\delta t_j + b_{2,j}\delta t_{j-1} + b_{3,j}\delta f_j + b_{4,j}\delta f_{j-1}\\
+b_{5,j}\delta g_j + b_{6,j}\delta g_{j-1} + b_{7,j}\delta p_j\\
b_{8,j}\delta p_{j-1} + b_{9,j}\delta n_j + b_{10,j}\delta n_{j-1}\\
+b_{11,j}\delta q_j + b_{12,j}\delta q_{j-1} = r_{6,j},\\
c_{1,j}\delta n_j + c_{2,j}\delta n_{j-1} + c_{3,j}\delta f_j + c_{4,j}\delta f_{j-1} +\\
c_{5,j}\delta t_j + c_{6,j}\delta t_{j-1} + c_{7,j}\delta s_j + c_{8,j}\delta s_{j-1} = r_{7,j},
\end{array}\right\} \tag{19}$$

herein

$$\left.\begin{array}{l}
a_{1,j} = 1 + \frac{\beta h_j}{8(\beta+1)}(N+1)(f_j+f_{j-1}),\\
a_{2,j} = a_{1,j} - 2.0,\\
a_{3,j} = \frac{\beta h_j}{8(\beta+1)}(N+1)(q_j+q_{j-1}),\\
a_{4,j} = a_{3,j},\\
a_{5,j} = \frac{-K\beta h_j}{2(\beta+1)} - \frac{M\beta h_j}{2(\beta+1)} - \frac{N\beta h_j}{2(\beta+1)}(p_j+p_{j-1}),\\
a_{6,j} = a_{5,j},
\end{array}\right\} \tag{20}$$

$$\left.\begin{array}{l}
b_{1,j} = 1 + \frac{3\,Pr\,h_j\,(N+1)}{8(3+4Rd)}(f_j+f_{j-1}) + \frac{3\,Pr\,N\,bh_j}{4(3+4Rd)}(n_j+n_{j-1})\\
+\frac{3\,Pr\,N\,th_j}{2(3+4Rd)}(t_j+t_{j-1})\\
b_{2,j} = b_{1,j} - 2.0,\\
b_{3,j} = \frac{3\,Pr\,h_j\,(N+1)}{8(3+4Rd)}(t_j+t_{j-1}),\\
b_{4,j} = b_{3,j},\\
b_{5,j} = \frac{3\lambda\,Pr\,h_j}{2(3+4Rd)},\\
b_{6,j} = b_{5,j},\\
b_{7,j} = \frac{3\,Pr\,J\,h_j}{2(3+4Rd)}(p_j) + \frac{3\,Pr\,J\,h_j}{2(3+4Rd)}(p_{j-1})\\
b_{8,j} = b_{7,j},\\
b_{9,j} = \frac{3\,Pr\,N\,bh_j}{4(3+4Rd)}(t_j) + \frac{3\,Pr\,N\,bh_j}{4(3+4Rd)}(t_{j-1}),\\
b_{10,j} = b_{9,j},\\
b_{11,j} = \frac{3\,Pr\,E\,ch_j(\beta+1)}{2\beta(3+4Rd)}(q_j+q_{j-1}),\\
b_{12,j} = b_{11,j},
\end{array}\right\} \tag{21}$$

$$\left.\begin{array}{l}
c_{1,j} = 1 + \frac{Sch_j(N+1)}{8}(f_j+f_{j-1}),\\
c_{2,j} = c_{1,j} - 2.0,\\
c_{3,j} = \frac{Sch_j}{8}(N+1)(n_j+n_{j-1}),\\
c_{4,j} = c_{3,j},\\
c_{5,j} = \frac{Nt}{Nb},\\
c_{6,j} = -\frac{Nt}{Nb},\\
c_{7,j} = -\frac{Sc\gamma h_j}{2},\\
c_{8,j} = c_{7,j},
\end{array}\right\} \tag{22}$$

$$\left.\begin{array}{l}
r_{1,j} = \frac{1}{2}\left(2(f_{j-1}-f_j) + h_j(p_j+p_{j-1})\right),\\
r_{2,j} = \frac{1}{2}\left(2(p_{j-1}-p_j) + h_j(q_j+q_{j-1})\right),\\
r_{3,j} = \frac{1}{2}\left(2(g_{j-1}-g_j) + +h_j(t_j+t_{j-1})\right),\\
r_{4,j} = \frac{1}{2}\left(2(s_{j-1}-s_j) + +h_j(n_j+n_{j-1})\right),\\
r_{5,j} = q_{j-1} - q_j - \frac{\beta h_j}{8(\beta+1)}(N+1)(f_j+f_{j-1})(q_j+q_{j-1})\\
+\frac{K\beta h_j}{2(\beta+1)}(p_j+p_{j-1}) + \frac{M\beta h_j}{2(\beta+1)}(p_j+p_{j-1})\\
+\frac{N\beta h_j}{4(\beta+1)}(p_j+p_{j-1})^2,\\
r_{6,j} = -t_j + t_{j-1} - \frac{3\,Pr\,h_j\,(N+1)}{8(3+4Rd)}(f_{j-1}+f_j)(t_{j-1}+t_j)\\
-\frac{3\lambda\,Pr\,h_j}{2(3+4Rd)}(g_{j-1}+g_j) - \frac{3\,Pr\,N\,bh_j}{4(3+4Rd)}(t_{j-1}+t_j)(n_{j-1}+n_j)\\
-\frac{3\,Pr\,N\,th_j}{4(3+4Rd)}(t_{j-1}+t_j)^2 - \frac{3\,Pr\,E\,ch_j(\beta+1)}{4\beta(3+4Rd)}(q_{j-1}+q_j)^2 +\\
-\frac{3\,Pr\,J\,h_j}{4(3+4Rd)}(p_{j-1}+p_j)^2,\\
r_{7,j} = n_{j-1} - n_j - \frac{Sch_j}{8}(N+1)(f_j+f_{j-1})(n_j+n_{j-1})\\
-\frac{Nt}{nb}(t_j-t_{j-1}) + \frac{Sc\gamma h_j}{2}(s_j+s_{j-1}).
\end{array}\right\} \tag{23}$$

The linear Eq. (17) resultant system is tackled by the Block elimination technique.

The system's equations in matrix form are:

$$\left.\begin{array}{c}[A_1][\delta_1]+[C_1][\delta_2]=[r_1],\\ [B_1][\delta_1]+[A_2][\delta_2]+[C_2][\delta_3]=[r_2],\\ [B_{j-1}][\delta_1]+[A_{j-1}][\delta_2]+[C_{j-1}][\delta_3]=[r_{j-1}],\\ [B_j][\delta_{j-1}]+[A_j][\delta_j]=[r_j],\end{array}\right\} \quad (24)$$

where,

$$A_1=\begin{bmatrix}0&0&0&1&0&0&0\\ -0.5h_j&0&0&0&-0.5h_j&0&0\\ 0&-0.5h_j&0&0&0&-0.5h_j&0\\ 0&0&-1&0&0&0&-0.5h_j\\ (a_2)_1&0&0&(a_3)_1&(a_1)_1&0&0\\ (b_{12})_1&(b_2)_1&0&(b_3)_1&(b_{11})_1&(b_1)_1&(b_9)_1\\ 0&(c_6)_1&(c_8)_1&(c_3)_1&0&(c_5)_1&(c_1)_1\end{bmatrix},$$

$$A_j=\begin{bmatrix}-0.5h_j&0&0&1&0&0&0\\ -1&0&0&0&-0.5h_j&0&0\\ 0&-1&0&0&0&-0.5h_j&0\\ 0&0&-1&0&0&0&-0.5h_j\\ (a_6)_j&0&0&(a_3)_j&(a_1)_j&0&0\\ (b_8)_j&(b_6)_j&0&(b_3)_j&(b_{11})_j&(b_1)_j&(b_9)_j\\ 0&0&(c_8)_j&(c_3)_j&0&(c_5)_j&(c_1)_j\end{bmatrix},$$

where, $2\le j\le J$,

$$B_j=\begin{bmatrix}0&0&0&-1&0&0&0\\ 0&0&0&0&-0.5h_j&0&0\\ 0&0&0&0&0&-0.5h_j&0\\ 0&0&0&0&0&0&-0.5h_j\\ 0&0&0&(a_4)_j&(a_2)_j&0&0\\ 0&0&0&(b_4)_j&(b_{12})_j&(b_2)_j&(b_{10})_j\\ 0&0&0&(c_4)_j&0&(c_6)_j&(c_2)_j\end{bmatrix},$$

where, $1\le j\le J-1$,

$$C_j=\begin{bmatrix}-0.5h_j&0&0&0&0&0&0\\ 1&0&0&0&0&0&0\\ 0&1&0&0&0&0&0\\ 0&0&1&0&0&0&0\\ (a_5)_j&0&0&0&0&0&0\\ (b_7)_j&(b_5)_j&0&0&0&0&0\\ 0&0&(c_7)_j&0&0&0&0\end{bmatrix}$$

where, $2\le j\le J$.

The LU decomposition method can work out the system's subsequent block diagonal form. The calculations are executed until the desired convergence criterion is met, and the calculations are terminated when the value of $\left|\delta g_0^{(i)}\right|<\varepsilon$, which is very small, reaches the recommended threshold.

4. OUTCOMES AND DISCUSSIONS

MATLAB plots temperature, velocity and concentration graphs to observe the impacts of different factors upon fluid flow upon a nonlinearly extended sheet. In Figure 2, we can see the velocity profile for dissimilar values of the porous media parameter, both with and without the presence of a magnetic field (M≠0 and M=0 cases). The highest velocity is observed when M=0, and it gradually decreases as the parameter K increases where the parameter K represents the resistance experienced by the fluid. As the value of K increases, the resistance for the fluid to flow through the porous medium is intensified, leading to a decrease in fluid velocity. When M≠0, the presence of the magnetic field introduces a frictional force known as the Lorentz force. This force opposes the fluid motion and further decreases the fluid velocity.

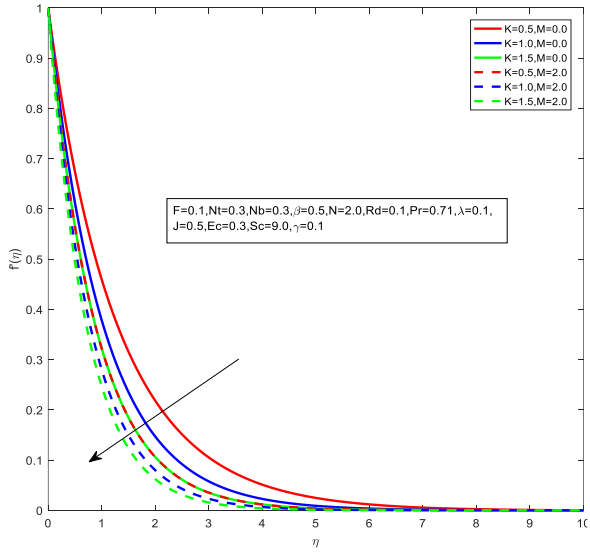

Figure 2. Velocity deviations of porosity parameter

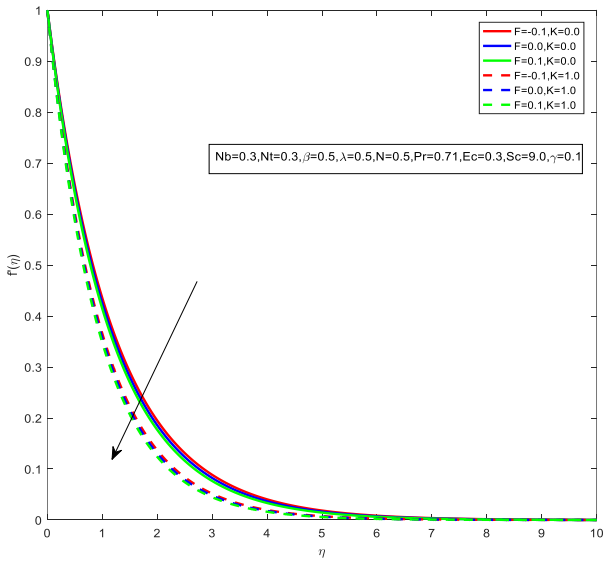

Figure 3. Velocity deviations of suction/injection parameter

Figure 3 represents the velocity distribution with $K\neq 0$ and without $K=0$ porous material's effects for the various approximated values of the suction/injection parameter. The plot demonstrates that fluid velocity rises with injection, drastically reducing as the suction parameter increases. This is due to the physical reality that the cold particles of the fluid are introduced into the micro-porous surface of the sheet via its cold surface. At the same time, the heated particles on the hot surface are pushed out of the micro-porous surface. This

weakens the convection current, and as a result, velocity decreases. It is further notable that the rapidity is highest, and the effects of K are more noticeable for $K = 0$ than from $K \neq 0$.

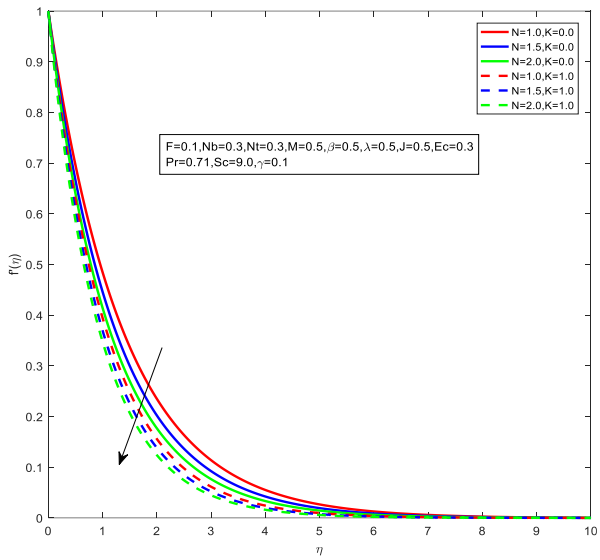

Figure 4. Velocity deviations of stretching parameter

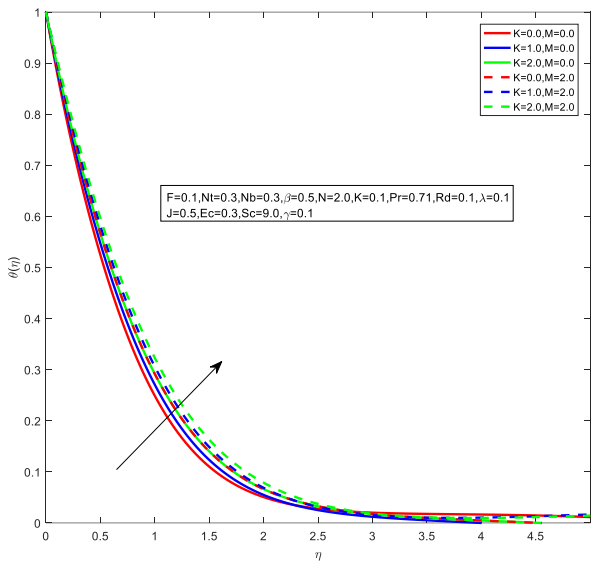

Figure 5. Temperature deviations of porosity parameter

Figure 4 represents velocity profiles for the diverse estimation of the stretching parameter n in both cases of the presence $(K \neq 0)$/absence $((K = 0))$ of a porous medium. It is perceived that velocity decays for higher estimations of N. Upon rising the parameter N, the boundary layer thickening reduces, and as a consequence, rapidity decreases. The thickness of the boundary layer is thinner for $K \neq 0$ than from $K = 0$. Figure 5 portrays the temperature profile for escalating estimations of the porous medium parameter with $M \neq 0$ and without $M = 0$ the occurrence of the magnetic field's impacts. The rise of porosity guides the escalation of the thermal boundary layer thickness, so the temperature of the liquid boosts. Also, the temperature is more for $M = 2$ than for $M = 0$. It is because the existence of a magneto force means the occurrence of the Lorentz force, which generates friction towards liquid, and as a cause, more heat is generated. Hence the resultant heat helps to grow the temperature.

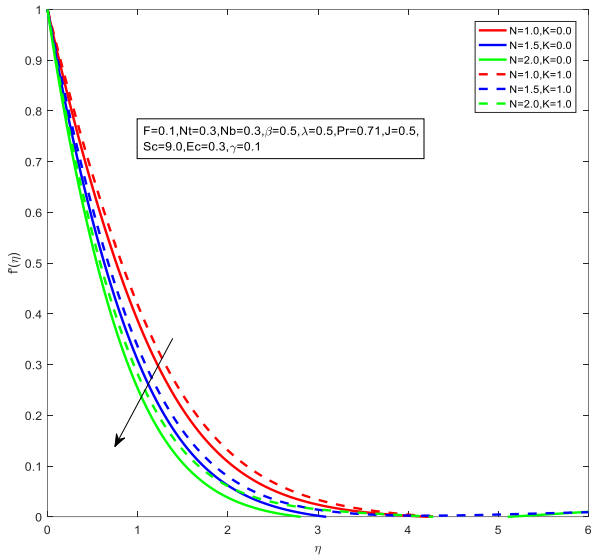

Figure 6. Temperature deviations of nonlinearity parameter

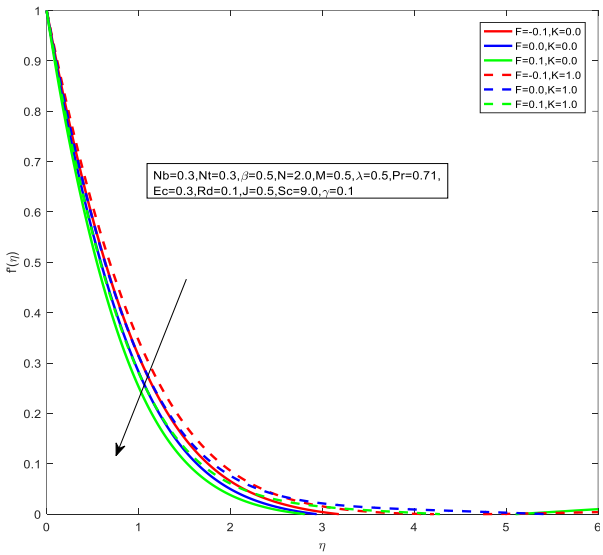

Figure 7. Temperature deviations of suction/injection parameter

Figure 6 represents temperature outlines of stretching parameter n in cases of presence $K \neq 0$ /absence $K = 0$ of porosity parameter. The temperature is observed to decline as the factor n grows, and this decrease is more for $K \neq 0$ than from $K = 0$. The escalation in the stretchable factor affects a deduction in the thermal boundary layer, which reduces the temperature.

Figure 7 represents temperature profiles for suction/injection parameter in the light and absence of porous material's effects, i.e., for $K \neq 1$ and $K = 0$. Growth in the suction parameter means an enhancement of fluid temperature. In contrast, a rise in the injection leads to a reduction in the temperature, and this reduction is more extensive for $K = 1$ than for $K = 0$.

Figure 8 portrays the temperature distribution for diverse estimations of radiation parameter. The temperature profile is observed elevated from $Rd = 0.5$ to $Rd = 2.0$. Enhancing the estimations of the radiation factor means the lessening in the mean absorbing factor, which indicates to the production of

more heat inside the fluid, so fluid temperature increases.

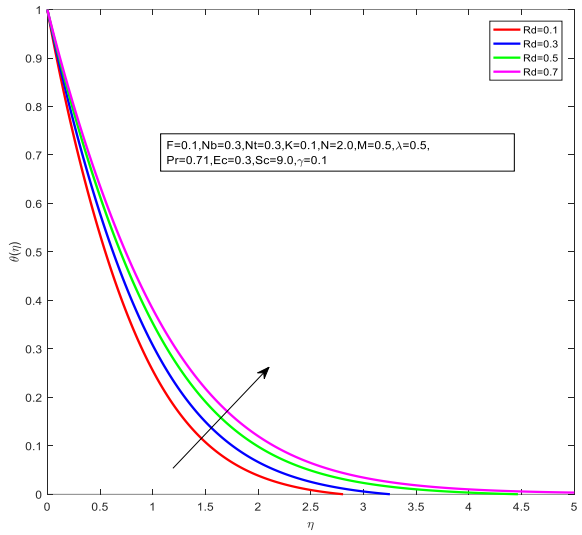

Figure 8. Temperature deviations of radiation parameter

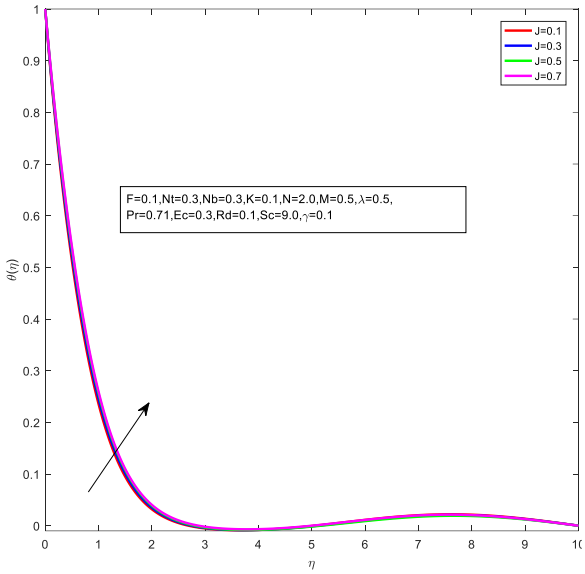

Figure 9. Temperature deviations of Joule heating parameter

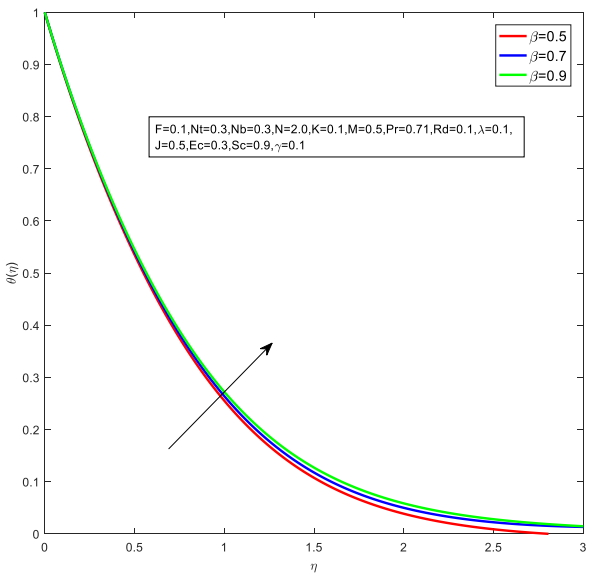

Figure 10. Temperature deviations of Casson parameter

In Figure 9, the temperature distribution due to Joule heating is presented. It is observed that as the Joule heating parameter (J) increases, the temperature in the conductor is enhanced. Higher values of the Joule heating parameter result in an increase in the temperature of the liquid, indicating a direct correlation between the parameter and the temperature rise.

Figure 10 illustrates the temperature outlines for different values of the Casson parameter variable. As the Casson variable (β) increases, the temperature is also observed to rise. This can be attributed to the fact that an increase in the β parameter leads to an increase in applied stress, this additionally increases the thickness of the temperature boundary layer. Consequently, the temperature increases.

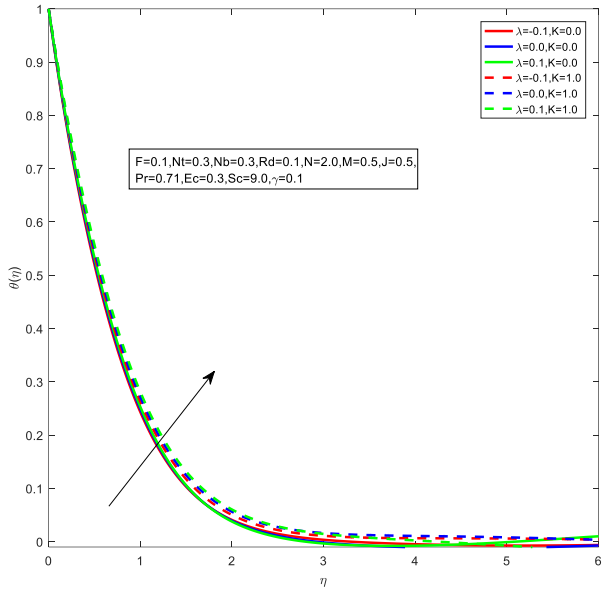

Figure 11. Temperature deviations of heat source parameter

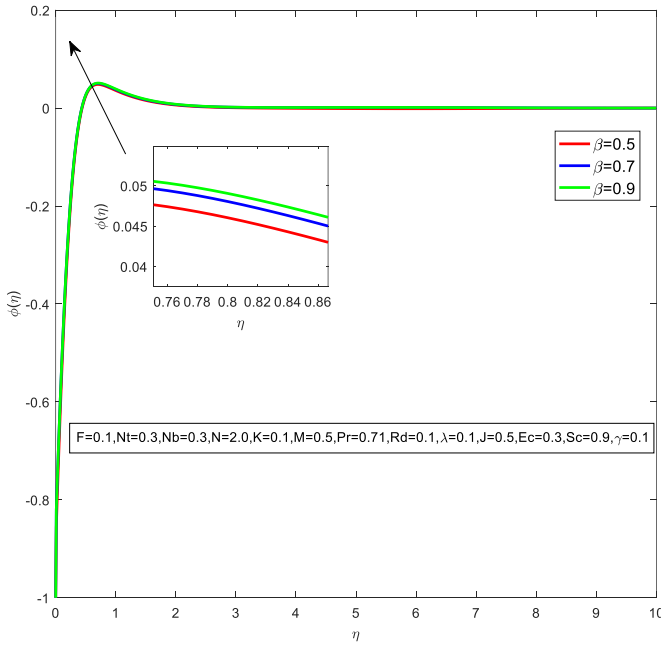

Figure 12. Concentration deviations of Casson parameter

Figure 11 displays the temperature outlines considering the heat source. By examining the graph for increasing values of the heat generating variable, it is evident that more heat is being added to the fluid. This additional heat input facilitates

an increase in the temperature and the temperature boundary layer.

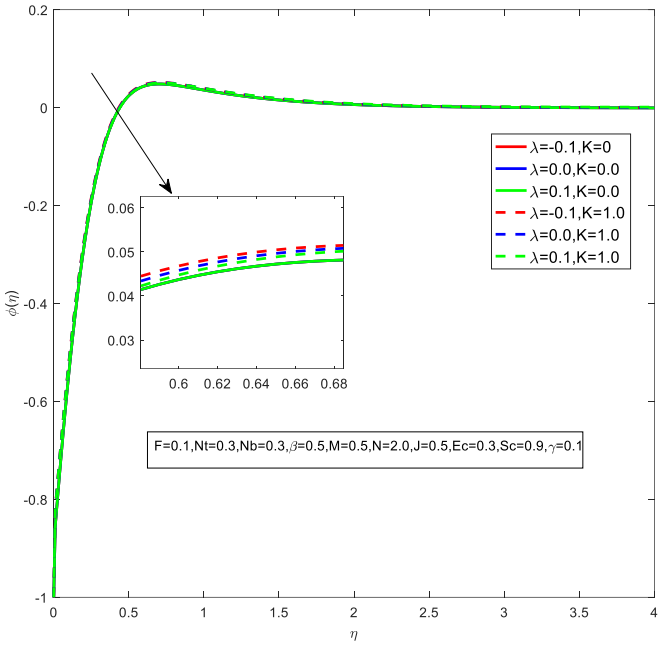

Figure 13. Concentration deviations of heat source parameter

Figure 12 portrays the concentration profile for the Casson parameter. The increasing observations of the Casson fluid parameter leads to growth in the viscosity and hence inner resistance of the fluid to flow. So, for enhanced estimations of the Casson liquid parameter, the concentration rises. Figure 13 represents the concentration profiles for the heat source parameter in the presence $(K = 1)$/absence $(K = 0)$ of the porosity parameter. It is noted that concentration downs with the rising observation of the heat source parameter, and this temperature falling is more extensive when $K = 0$.

Table 1 represents skin friction drag values for diverse values of n and K in suction and injection cases. It is perceived that more frictional force will be generated for higher observations of K. Table 2 represents the Nusselt number for progressive observations of K and Nt regarding the Prandtl number and distinct values of Ec and γ. For higher values of K in both situations of sucking (injection). It is witnessed that the Nusselt number rises. Table 3 represents Sherwood numbers for progressive values of chemical reaction parameter, also for progressive values of K, Nt, and concerning Prandtl number. Table 4 presents a comparative study of the Nusselt number for different values of the Prandtl number. It is observed that as the Prandtl number increases, the Nusselt number also increases. This finding is consistent with previous studies and aligns well with the existing literature, indicating a good agreement (Table 5).

Table 1. Estimations of $f''(0)$ for distinct values of n, K

n	*F*	*K*	$f''(0)$
1	-0.2	1	0.698437
2	-0.2	2	0.839000
3	-0.2	3	0.938807
1	0.2	1	0.744031
2	0.2	2	0.901365
3	0.2	3	1.015967

Table 2. Values of -$\theta'(0)$

Pr	*Sc*	*Ec*	*β*	*λ*	*n*	*γ*	*M*	*F*	*K*	*Nb*	*Nt*	*Rd*	*J*	-$\theta'(0)$
7	9	0.1	0.5	0.2	2	0.1	1	0.2	2	0.3	0.3	0.1	0.1	0.753804
		0.2				0.5								0.733717
		0.3				1.0								0.680683
0.7	9	0.3	0.5	0.2	2	0.1	1	0.2	0.0	0.1	0.1	0.1	0.1	0.491388
0.7									1.0		0.2			0.402130
0.7									2.0		0.3			0.297585
1.0									0.0		0.1			0.562524
1.0									1.0		0.2			0.466578
1.0									2.0		0.3			0.352080
7	9	0.3	0.5	0.2	1.0	0.1	1	-0.2	0.0	0.1	0.3	0.1	0.1	0.219967
								-0.2	1.0					0.204350
								-0.2	2.0					0.092368
								0.2	0.0					0.369446
								0.2	1.0					0.243694
								0.2	2.0					0.061423

Table 3. Values of -$\phi'(0)$

Pr	*Sc*	*Ec*	*β*	*λ*	*n*	*γ*	*M*	*F*	*K*	*Nb*	*Nt*	*Rd*	*J*	-$\phi'(0)$
7	9	0.3	0.5	0.2	2	0.0	1	0.2	2	0.1	0.1	0.1	0.1	-0.022872
						0.1								-0.450766
						0.3								-0.673748
1	9	0.3	0.5	0.2	2	0.1	1	0.2	0.0	0.1	0.1	0.1	0.1	-0.518578
									1.0		0.3			-1.563202
									2.0		0.5			-2.138776
0.7	9	0.3	0.5	0.2	2	0.1	1	0.2	0.0	0.1	0.1	0.1	0.1	-0.516875
									1.0		0.3			-1.557335
									2.0		0.5			-2.157702
								0.2	2.0					0.061423

Table 4. Comparative study of $-\theta'(0)$

Pr	Bachok et al. [32]	Abo-dahab et al. [41]	Present Results
5.0	2.43078	2.43075	2.43665
7.0	2.85270	2.85266	2.82272
9.0	3.21459	3.21451	3.27122

Table 5. Thermophysical properties of nanofluid

Property	Nanofluid
Density	$\rho_{nf} = (1-\varphi_1)\rho_f + \varphi_1\rho_{s_1}$
Viscosity	$\mu_{nf} = \frac{\mu_f}{(1-\varphi_1)^{2.5}}$
Thermal Conductivity	$k_{nf} = \frac{k_{s_1} + 2k_f - 2\varphi_1\left(k_f - k_{s_1}\right)}{k_{s_1} + 2k_f + \varphi_1\left(k_f - k_{s_1}\right)} k_f$

5. CONCLUSIONS

The present study shows MHD Casson-type nanofluid movement via a nonlinearly stretchable plate along with suction/injection. Also, Joule heating, and radiation influences are considered. Fluid flow is across a porous material. The chemical reaction is also taken into consideration. Flow due to a nonlinearly stretching sheet has potential applications in various fields of science, such as metallurgy and chemical engineering processes with industrial applications which include glass fibre, paper production, hot rolling, metal spinning, wire drawing, etc.

It is determined that:

- The liquid flowing rapidity is reduced in the presence of the absorbent medium, suction/injection, and non-linear stretching parameter.
- The fluid temperature is enhanced in case of progressive observations of Casson, radiation, Joule heating, and heat source parameters. The opposite nature is detected in the nonlinearly stretching parameters.
- The fluid concentration is increased for the Casson factor and decayed for heat source variable.
- Fluid viscosity and thermal radiation, chemical reaction, porosity and Joule heating have significant impact on the Casson nanofluid flow.
- The remarkable phenomenon of Joule heating effect finds its applications in diverse industries such as food processing, materials synthesis, medicine, pharmacology, and chemical industries. By harnessing the power of Joule heating, we can ensure the maintenance of high-quality food products and facilitate the synthesis and processing of various materials.
- In future this work can be carried out for new types of flow flat forms, adding few more effects and different types of Nano fluids. Also, this study can be extended for hybrid Nano fluids.

REFERENCES

[1] Choi, S.U.S., Eastman, J.A. (1995). Enhancing thermal conductivity of fluids with nanoparticles. In Proceedings of the 1995 ASME International Mechanical Engineering Congress and Exposition, San Francisco, CA, USA. https://www.osti.gov/servlets/purl/196525.

[2] Al-Chlaihawi, K.K., Alaydamee, H.H., Faisal, A.E., Al-Farhany, K., Alomari, M.A. (2022). Newtonian and non-Newtonian nanofluids with entropy generation in conjugate natural convection of hybrid nanofluid-porous enclosures: A review. Heat Transfer, 51(2): 1725-1745. https://doi.org/10.1002/htj.22372

[3] Abdulsahib, A.D., Al-Farhany, K. (2021). Review of the effects of stationary/rotating cylinder in a cavity on the convection heat transfer in porous media with/without nanofluid. Math. Mathematical Modelling of Engineering Problems, 8(3): 356-364. https://doi.org/10.18280/mmep.080304

[4] Redouane, F., Jamshed, W., Devi, S.S.U., Amine, B.M., Safdar, R., Al-Farhany, K., Eid, M.R., Nisar, K.S., Abdel-Aty, A.H., Yahia, I.S. (2021). Influence of entropy on Brinkman–Forchheimer model of MHD hybrid nanofluid flowing in enclosure containing rotating cylinder and undulating porous stratum. Scientific Reports, 11: 24316. https://doi.org/10.1038/s41598-021-03477-4

[5] Sridhar, W., Lakshmi, G.V., Al-Farhany, K., Ganesh, G.R. (2021). MHD Williamson nanofluid across a permeable medium past an extended sheet with constant and irregular thickness. Heat Transfer, 50(8): 8134-8154. https://doi.org/10.1002/htj.22270

[6] Li, Q., Xuan, Y.M. (2002). Convective heat transfer and flow characteristics of Cu-water nanofluid. Science in China Series E: Technolgical Science, 45: 408-416. https://doi.org/10.1360/02ye9047

[7] Kang, H.U., Kim, S.H., Oh, J.M. (2006). Estimation of thermal conductivity of nanofluid using experimental effective particle volume. Experimental Heat Transfer, 19(3): 181-191. https://doi.org/10.1080/08916150600619281

[8] Jang, S.P. Choi, S.U.S. (2007). Effects of various parameters on nanofluid thermal conductivity. Journal of Heat and Mass Transfer, 129(5): 617-623. https://doi.org/10.1115/1.2712475

[9] Yu, W.H., France, D.M., Routbort, J.L. (2008). Review and comparison of nanofluid thermal conductivity and heat transfer enhancements. Heat Transfer Engineering, 29(5): 432-460. https://doi.org/10.1080/01457630701850851

[10] Anoop, K.B., Sundararajan, T., Das, S.K. (2009). Effect of particle size on the convective heat transfer in nanofluid in the developing region. International Journal of Heat and Mass Transfer, 52(9-10): 2189-2195. https://doi.org/10.1016/j.ijheatmasstransfer.2007.11.063

[11] Dash, R.K., Mehta, K.N., Jayaraman, G. (1996). Casson fluid flow in a pipe filled with a homogeneous porous medium. International Journal of Engineering Science, 34(10): 1145-1156. https://doi.org/10.1016/0020-7225(96)00012-2

[12] Hady, F.M., Ibrahim, F.S., Abdel-Gaied, S.M., Eid, M.R. (2012). Radiation effect on viscous flow of a nanofluid and heat transfer over a nonlinearly stretching sheet. Nanoscale Research Letters, 7: 229. https://doi.org/10.1186/1556-276X-7-229

[13] Nadeem, S., Haq, R.U., Lee, C. (2012). MHD flow of a Casson fluid over an exponentially shrinking sheet. Scientia Iranica, 19(6): 1550-1553. https://doi.org/10.1016/j.scient.2012.10.021

[14] Mukhopadhyay, S., De, P.R., Bhattacharyya, K., Layek, G.C. (2013). Casson fluid flow over an unsteady

stretching surface. Ain Shams Engineering Journal, 4(4): 933-938. https://doi.org/10.1016/j.asej.2013.04.004
[15] Swati, M. (2013). Casson fluid flow and heat transfer over a nonlinearly stretching surface. Chinese Physics B, 22(7): 074701. https://doi.org/10.1088/1674-1056/22/7/074701
[16] Shehzad, S.A., Hayat, T., Qasim, M., Asghar, S. (2013). Effects of mass transfer on MHD flow of Casson fluid with chemical reaction and suction. Brazilian Journal of Chemical Engineering, 30(1): 187-195. https://doi.org/10.1590/S0104-66322013000100020
[17] Mukhopadhyay, S., Mondal, I.C., Chamkha, A.J. (2013). Casson fluid flow and heat transfer past a symmetric wedge. Heat Transfer, 42(8): 665-675. https://doi.org/10.1002/htj.21065
[18] Pramanik, S. (2014). Casson fluid flow and heat transfer past an exponentially porous stretching surface in presence of thermal radiation. Ain Shams Engineering Journal, 5(1): 205-212. https://doi.org/10.1016/j.asej.2013.05.003
[19] Sheikholeslami, M., Ganji, DD., Javed, M.Y., Ellahi, R. (2015). Effect of thermal radiation on magnetohydrodynamics nanofluid flow and heat transfer by means of two phase model. Journal of Magnetism and Magnetic Materials, 374: 36-43. https://doi.org/10.1016/j.jmmm.2014.08.021
[20] Haq, R.U., Nadeem, S., Khan, Z.H., Akbar, N.S. (2015). Thermal radiation and slip effects on MHD stagnation point flow of nanofluid over a stretching sheet. Physica E: Low-dimensional Systems and Nanostructures, 65: 17-23. https://doi.org/10.1016/j.physe.2014.07.013
[21] Hussain, T., Shehzad, S.A., Alsaedi, A., Hayat, T., Ramzan, M. (2015). Flow of Casson nanofluid with viscous dissipation and convective conditions: A mathematical model. Journal of Central South University, 22: 1132-1140. https://doi.org/10.1007/s11771-015-2625-4
[22] Hayat, T., Asad, S., Alsaedi, A. (2016). Flow of Casson fluid with nanoparticles. Applied Mathematics and Mechanics, 37: 459-470. https://doi.org/10.1007/s10483-016-2047-9
[23] Ibrahim, W., Makinde, O.D. (2015). Magnetohydrodynamic stagnation point flow and heat transfer of Casson nanofluid past a stretching sheet with slip and convective boundary condition. Journal of Aerospace Engineering, 29(2): 04015037. https://doi.org/10.1061/(ASCE)AS.1943-5525.0000529
[24] Ullah, I., Khan, I., Shafie, S. (2016). MHD natural convection flow of Casson nanofluid over nonlinearly stretching sheet through porous medium with chemical reaction and thermal radiation. Nanoscale Research Letters, 11: 527. https://doi.org/10.1186/s11671-016-1745-6
[25] Kataria, H.R, Patel, H.R. (2016). Radiation and chemical reaction effects on MHD Casson fluid flow past an oscillating vertical plate embedded in porous medium. Alexandria Engineering Journal, 55(1): 583-595. https://doi.org/10.1016/j.aej.2016.01.019
[26] Qing, J., Bhatti, M.M., Abbas, M.A., Rashidi, M.M., Ali, M.E.S. (2016). Entropy generation on MHD Casson nanofluid flow over a porous stretching/shrinking surface. Entropy 18(4): 123. https://doi.org/10.3390/e18040123
[27] Zaib, A., Rashidi, M.M., Chamkha, A.J., Al-Mudhaf, A.F. (2017). Nonlinear radiation effect on Casson nanofluid past a plate immersed in Darcy–Brinkman porous medium with binary chemical reaction and activation energy. International Journal of Fluid Mechanics Research, 44(6): 513-531. https://doi.org/10.1615/InterJFluidMechRes.2017019749
[28] Naqvi, S.M.R.S., Muhammad, T., Asma, M. (2020). Hydromagnetic flow of Casson nanofluid over a porous stretching cylinder with Newtonian heat and mass conditions. Physica A: Statistical Mechanics and its Applications, 550: 123988. https://doi.org/10.1016/j.physa.2019.123988
[29] Hossain, M.A. (1992). Viscous and Joule heating effects on MHD free convection flow with variable plate temperature. International Journal of Heat and Mass Transfer, 35(12): 3485-3487. https://doi.org/10.1016/0017-9310(92)90234-J
[30] Chen, C.H. (2010). Combined effects of Joule heating and viscous dissipation on magnetohydrodynamic flow past a permeable, stretching surface with free convection and radiative heat transfer. Journal of Heat and Mass Transfer, 132(6): 064503. https://doi.org/10.1115/1.4000946
[31] Hayat, T., Qasim, M. (2010). Influence of thermal radiation and Joule heating on MHD flow of a Maxwell fluid in the presence of thermophoresis. International Journal of Heat and Mass Transfer, 53(21-22): 4780-4788. https://doi.org/10.1016/j.ijheatmasstransfer.2010.06.014
[32] Bachok, N., Ishak, A., Pop, I. (2010). Boundary-layer flow of nanofluids over a moving surface in a flowing fluid. International Journal of Thermal Sciences, 49(9): 1663-1668. https://doi.org/10.1016/j.ijthermalsci.2010.01.026
[33] Chamkha, A.J., Mohamed, R.A., Ahmed, S.E. (2011). Unsteady MHD natural convection from a heated vertical porous plate in a micropolar fluid with Joule heating, chemical reaction and radiation effects. Meccanica, 46: 399-411. https://doi.org/10.1007/s11012-010-9321-0
[34] Hayat, T., Shafiq, A., Alsaedi, A. (2014). Effect of Joule heating and thermal radiation in flow of third grade fluid over radiative surface. Plos One, 9(1): e83153. https://doi.org/10.1371/journal.pone.0083153
[35] Kempannagari, A.K., Buruju, R.R., Naramgari, S., Vangala, S. (2020). Effect of Joule heating on MHD non-Newtonian fluid flow past an exponentially stretching curved surface. Heat Transfer, 49(6): 3575-3592. https://doi.org/10.1002/htj.21789
[36] Wakif, A., Animasaun, I.L., Narayana, P.V.S., Sarojamma, G. (2020). Meta-analysis on thermo-migration of tiny/nano-sized particles in the motion of various fluids. Chinese Journal of Physics, 68: 293-307. https://doi.org/10.1016/j.cjph.2019.12.002
[37] Wakif, A., Chamkha, A., Thumma, T., Animasaun, I.L., Sehaqui, R. (2021). Thermal radiation and surface roughness effects on the thermo-magneto-hydrodynamic stability of alumina-copper oxide hybrid nanofluids utilizing the generalized Buongiorno's nanofluid model. Journal of Thermal Analysis and Calorimetry, 143: 1201-1220. https://doi.org/10.1007/s10973-020-09488-z.
[38] Ganesh, G.R., Sridhar, W. (2022). Effect of chemical reaction towards MHD marginal layer movement of Casson nanofluid through porous media above a moving plate with an adaptable thickness. Pertanika Journal of

Science and Technology, 30(1): 477-495. https://doi.org/10.47836/pjst.30.1.26
[39] BalajiPrakash, G., Gurrampati, V.R.R., Sridhar, W., Krishna, Y.H., Mahaboob, B. (2019). Thermal radiation and heat source effects on MHD Casson fluid over an oscillating vertical porous plate. Journal of Computer and Mathematical Sciences, 10(5): 1021-1031. https://doi.org/10.29055/jcms/1088
[40] Ganesh, G.R., Sridhar, W. (2021). MHD radiative Casson—nanofluid stream above a nonlinear extending surface including chemical reaction through Darcy-Forchiemer medium. Heat Transfer, 50(8): 7691-7711. https://doi.org/10.1002/htj.22249
[41] Abo-Dahab, S.M., Abdelhafez, M.A., Mebarek-Oudina, F., Bilal, S.M. (2021). MHD Casson nanofluid flow over nonlinearly heated porous medium in presence of extending surface effect with suction/injection. Indian Journal of Physics, 95: 2703-2717. https://doi.org/10.1007/s12648-020-01923-z
[42] Rasool, G., Wakif, A. (2021). Numerical spectral examination of EMHD mixed convective flow of second-grade nanofluid towards a vertical Riga plate using an advanced version of the revised Buongiorno's nanofluid model. Journal of Thermal Analysis and Calorimetry, 143: 2379-2393. https://doi.org/10.1007/s10973-020-09865-8
[43] Wakif, A., Animasaun, I.L., Khan, U., Shah, N.A., Thumma, T. (2021). Dynamics of radiative-reactive Walters-B fluid due to mixed convection conveying gyrotactic microorganisms, tiny particles experience haphazard motion, thermo-migration, and Lorentz force. Physica Scripta, 96(12): 125239. https://doi.org/10.1088/1402-4896/ac2b4b
[44] Wakif, A., Animasaun, I.L., Sehaqui, R. (2021). A brief technical note on the onset of convection in a horizontal nanofluid layer of finite depth via wakif-Galerkin weighted residuals technique (WGWRT). Defect and Diffusion Forum, 409: 90-94. https://doi.org/10.4028/www.scientific.net/DDF.409.90
[45] Gumber, P., Yaseen, M., Rawat, S.K., Kumar, M. (2022). Heat transfer in micropolar hybrid nanofluid flow past a vertical plate in the presence of thermal radiation and suction/injection effects. Partial Differential Equations in Applied Mathematics, 5: 100240. https://doi.org/10.1016/j.padiff.2021.100240
[46] Ganesh, G.R., Sridhar, W., Talla, H., Deevi, S.K. (2020). Forced convection heat transfer of MHD Casson fluid in non darcy porous media. International Journal of Advanced Science and Technology, 29(6): 1313-1326.
[47] Sridhar, W., Ganesh, G.R., Rao, B.V.A., Gorfie, E. (2021). Mixed convection boundary layer flow of MHD Casson fluid on an upward stretching sheet encapsulated in a porous medium with slip effects. JP Journal of Heat and Mass Transfer, 22(2): 133-149. https://doi.org/10.17654/HM022020133
[48] Wakif, A., Zaydan, M., Alshomrani, A.S., Muhammad, T., Sehaqui, R. (2022). New insights into the dynamics of alumina-(60% ethylene glycol + 40% water) over an isothermal stretching sheet using a renovated Buongiorno's approach: A numerical GDQLLM analysis. International Communications in Heat and Mass Transfer, 133: 105937. https://doi.org/10.1016/j.icheatmasstransfer.2022.105937
[49] Wakif, A., Abderrahmane, A., Guedri K., Bouallegue, B., Kaewthongrach, R., Kaewmesri, P., Jirawattanapanit, A. (2022). Importance of exponentially falling variability in heat generation on chemically reactive von Kármán nanofluid flows subjected to a radial magnetic field and controlled locally by zero mass flux and convective heating conditions: Differential quadrature. Frontiers in Physics, 10: 988275. https://doi.org/10.3389/fphy.2022.988275
[50] Wakifa, A., Shahb, N.A. (2022). Hydrothermal and mass impacts of azimuthal and transverse components of Lorentz forces on reacting Von Kármán nanofluid flows considering zero mass flux and convective heating conditions. Waves in Random and Complex Media, 1-22. https://doi.org/10.1080/17455030.2022.2136413
[51] Ghadikolaei, S.S., Gholinia, M. (2019). Terrific effect of H2 on 3D free convection MHD flow of C2H6O2H2O hybrid base fluid to dissolve Cu nanoparticles in a porous space considering the thermal radiation and nanoparticle shapes effects. International Journal of Hydrogen Energy, 44(31): 17072-17083. https://doi.org/10.1016/j.ijhydene.2019.04.171
[52] Gulzar, M.M., Aslam, A., Waqas, M., Javed, M.A., Hosseinzadeh, K. (2020). A nonlinear mathematical analysis for magneto-hyperbolic-tangent liquid featuring simultaneous aspects of magnetic field, heat source and thermal stratification. Applied Nanoscience, 10: 4513-4518. https://doi.org/10.1007/s13204-020-01483-y
[53] Ghadikolaei, S.S., Gholinia, M. (2020). 3 D mixed convection MHD flow of GO-MoS2 hybrid nanoparticles in H2O–(CH2OH)2 hybrid base fluid under the effect of H2 bond. International Communications in Heat and Mass Transfer, 110: 104371. https://doi.org/10.1016/j.icheatmasstransfer.2019.104371
[54] Ghadikolaei, S.S.C. (2021). An enviroeconomic review of the solar PV cells cooling technology effect on the CO_2 emission reduction. Solar Energy, 216: 468-492. https://doi.org/10.1016/j.solener.2021.01.016
[55] Ghadikolaei, S.S.C. (2021). Solar photovoltaic cells performance improvement by cooling technology: An overall review. International Journal of Hydrogen Energy, 46(18): 10939-10972. https://doi.org/10.1016/j.ijhydene.2020.12.164
[56] Akbari, S., Faghiri, S., Poureslami, P., Hosseinzadeh, K., Shafii, M.B. (2022). Analytical solution of non-Fourier heat conduction in a 3-D hollow sphere under time-space varying boundary conditions. Heliyon, 8(12): e12496. https://doi.org/10.1016/j.heliyon.2022.e12496
[57] Siahchehrehghadikolaei, S., Gholinia, M., Ghadikolaei, S.S., Lin, C.X. (2022). A CFD modeling of CPU cooling by eco-friendly nanofluid and fin heat sink passive cooling techniques. Advanced Powder Technology, 33(11): 103813. https://doi.org/10.1016/j.apt.2022.103813
[58] Faghiri, S., Akbari, S., Shafii, M.B., Hosseinzadeh, K. (2022). Hydrothermal analysis of non-Newtonian fluid flow (blood) through the circular tube under prescribed non-uniform wall heat flux. Theoretical and Applied Mechanics Letters, 12(4): 100360. https://doi.org/10.1016/j.taml.2022.100360
[59] Rostami, H.T., Najafabadi, M.F., Hosseinzadeh, K., Ganji, D.D. (2022). Investigation of mixture-based dusty

hybrid nanofluid flow in porous media affected by magnetic field using RBF method. International Journal of Ambient Energy, 43(1): 6425-6435. https://doi.org/10.1080/01430750.2021.2023041

[60] Attar, M.A., Roshani, M., Hosseinzadeh, K., Ganji, D.D. (2022). Analytical solution of fractional differential equations by Akbari–Ganji's method. Partial Differential Equations in Applied Mathematics, 6: 100450. https://doi.org/10.1016/j.padiff.2022.100450

[61] Najafabadi, M.F., Rostami, H.T., Hosseinzadeh, K., Ganji, D.D. (2022). Hydrothermal study of nanofluid flow in channel by RBF method with exponential boundary conditions. Proceedings of the Institution of Mechanical Engineers, Part E: Journal of Process Mechanical Engineering, 095440892211339. https://doi.org/10.1177/09544089221133909

[62] Zangooee, M.R., Hosseinzadeh, K., Ganji, D.D. (2022). Hydrothermal analysis of hybrid nanofluid flow on a vertical plate by considering slip condition. Theoretical and Applied Mechanics Letters, 12(5): 100357. https://doi.org/10.1016/j.taml.2022.100357

[63] Ghadikolaei, S.S., Siahchehrehghadikolaei, S., Gholinia, M., Rahimi, M. (2023). A CFD modeling of heat transfer between CGNPs/H_2O Eco-friendly nanofluid and the novel nature-based designs heat sink: Hybrid passive techniques for CPU cooling. Thermal Science and Engineering Progress, 37: 101604. https://doi.org/10.1016/j.tsep.2022.101604

[64] Hosseinzadeh, K., Mardani, M.R., Paikar, M., Hasibi, A., Tavangar, T., Nimafar, M., Ganji, D.D., Shafii, M.B. (2023). Investigation of second grade viscoelastic non-Newtonian nanofluid flow on the curve stretching surface in presence of MHD. Results in Engineering, 17: 100838. https://doi.org/10.1016/j.rineng.2022.100838

NOMENCLATURE

u, v	rapidity elements in x, y orientation
u_w	stretching sheet velocity
T_w	temperature of stretching sheet
T_∞	ambient temperature
C_∞	ambient concentration
υ	kinematic viscosity($m^2\ s^{-1}$)
β	Casson liquid variable
k_0	permeability of the porous material
σ	electrical conductivity(s/m)
$B(x)$	magnetic field's strength(N/m/a)
ρ_f	fluid viscosity
T	temperature of nanofluid
α	thermal diffusivity(m^2/s)
Pr	Prandtl quantity
λ	heat source or sink parameter
Ec	Eckert number
J	Joule heating parameter
F	suction/injection parameter
C_{fx}	skin friction parameter
τ_w	shear stress
Q_0	heat source parameter
c_p	specific heat capacitance ($J\ k\ g^{-1}\ K^{-1}$)
τ	ratio of heat capacity
D_T	thermophoretic parameter
D_B	Brownian motion factor
q_r	radiative heat flux
k_1	chemical reaction coefficient
a, A	constants
k	thermal conductivity($Wm^{-1}K^{-1}$)
N	nonlinearity parameter
K	porous medium argument
M	magnetic parameter
Rd	radiation parameter
Nb	Brownian motion argument
Nt	thermophoretic argument
Sc	Schmidt number
γ	chemical reaction parameter
Nu_x	local nusselt number
Sh_x	local sherwood number
q_w, q_m	wall heat and mass flux

Abbreviations

PDE	partial differential equations
ODE	ordinary differential equations